J. Fluid Mech. (2004), *vol.* 511, *pp.* 363–379.
DOI: 10.1017/S0022112004009668 Printed in the United Kingdom

The wall-jetting effect in Mach reflection: Navier–Stokes simulations

By E. I. VASILEV[1], G. BEN-DOR[2], T. ELPERIN[2] AND L. F. HENDERSON[2]

[1]Department of Computational Mechanics, Volgograd State University, Volgograd, Russia

[2]Pearlstone Center for Aeronautical Engineering Studies, Department of Mechanical Engineering, Ben-Gurion University of the Negev, Beer Sheva, Israel

(Received 19 May 2003 and in revised form 2 April 2004)

The wall-jetting effect in Mach reflections in viscous pseudo-steady flows (as obtained in shock tubes) is investigated numerically. The W-modification of Godunov's scheme has been modified to solve the Navier–Stokes equations using a splitting into physical processes. The viscous terms are approximated using an explicit scheme with central differences in space and a two-step Runge–Kutta method in time. Two analytical models are considered. The first is a self-similar viscous flow model in which we consider a flow field with characteristic size L, and assume that as the characteristic size grows from 0 to L, the viscosity of the gas ahead of the shock wave varies from 0 to μ_0. Consequently, the flow can be made self-similar by using the parameter $Re = \rho_0 a_0 L/\mu_0$. The second is a real non-stationary viscous flow, in which the molecular viscosity during the growth of a characteristic size from 0 to L remains constant and is equal μ_0. As a result the viscous effects are only partially accounted for in the self-similar viscous flow model in comparison to a real non-stationary viscous flow model, since they are smaller in the former case. The present investigation complements our previous investigation of the wall-jetting effect in Mach reflection in inviscid pseudo-steady flows (Henderson *et al.* 2003).

1. Introduction

The non-stationary reflection of a plane shock wave over a straight wedge has been investigated quite extensively in the past four decades. Details on this type of reflection can be found in Ben-Dor (1991). The state of knowledge regarding the transition criteria between the various types of reflection wave configurations is summarized in Li & Ben-Dor (1995). Under the assumption that the fluid is inviscid the flow field can be regarded as self-similar (see e.g. Jones *et al.* 1951). The solutions of the Euler equations for this case are stationary (pseudo-stationary) in a frame of reference attached to the incident shock wave. Using an inviscid model, Henderson *et al.* (2003) showed, in the course of their numerical investigation of the jetting phenomenon in Mach reflection, that these stationary self-similar solutions could become unstable, and as a result the flow field could become time-dependent. Henderson *et al.* (2003) also showed that this instability-driven non-stationarity has usually a local oscillatory character, i.e. it manifests itself only in certain regions of the flow field.

In the present study the simplifying assumption of an inviscid flow is removed and a more realistic model that accounts for the viscosity is used. Consequently, the Navier–Stokes rather than the Euler equations are solved numerically. Owing to the

fact that the characteristic size of the flow field, L, grows linearly with time $L \sim Dt$ (where D is the velocity of the incident shock wave) the Reynolds number, i.e. the ratio of the convective term to the viscous term, varies with time too.

Therefore, when the viscosity is accounted for, the problem must be formulated as a non-stationary one from the very beginning. However, this non-stationary flow can become unstable also, and similarly to the jetting phenomenon in the case of inviscid flows, fluctuations of the flow parameters could occur due to local instabilities, e.g. in the wall-jet.

Clearly, it is worthwhile to separate these two factors in the case of non-stationary flows, and study them separately. This indeed is done in the present study by using a *self-similar viscous flow model.*

In the self-similar viscous flow model we consider a flow field with a characteristic size L, and assume that as the characteristic size grows from 0 to L, the viscosity of the gas ahead of the shock wave varies from 0 to μ_0. Consequently, the flow can be made self-similar by using the parameter $Re = \rho_0 a_0 L/\mu_0$, where ρ_0 and a_0 are respectively the density and the speed of sound of the gas ahead of the shock wave. Note that while in the real *non-stationary viscous flow*, the molecular viscosity during the growth of a characteristic size from 0 to L remains constant and is equal μ_0, in the model of self-similar viscous flow it grows from 0 to μ_0. As a result the viscosity is smaller in the self-similar viscous flow model than in the real non-stationary viscous flow model. Hence, the viscous effects are only partially accounted for in the self-similar viscous flow in comparison to a real non-stationary viscous flow. Therefore, in the range of Reynolds numbers in which a self-similar viscous flow is stable, the non-stationary viscous flow is also stable. Also, by comparing the solutions of the non-stationary and the self-similar viscous flow cases one can estimate the effect of the non-stationarity that results from variations in the Reynolds number during the evolution of the flow.

2. The governing equations and the numerical method

We consider a plane incident shock in a perfect gas ($\gamma = 1.4$), with Mach number $M_i = D/a_0$, diffracting over a wedge of angle θ_w. The problem was analysed by numerically solving the following system of mass, momentum (Navier–Stokes) and energy conservation equations for a viscous heat conducting gas:

$$\rho_t + \nabla \cdot (\rho \boldsymbol{v}) = 0, \tag{1a}$$

$$(\rho \boldsymbol{v})_t + \nabla \cdot (\rho \boldsymbol{v}\boldsymbol{v}) + \nabla p = \nabla \cdot \boldsymbol{\tau}, \tag{1b}$$

$$E_t + \nabla \cdot [(E + p)\boldsymbol{v}] = \nabla \cdot (\boldsymbol{\tau} \cdot \boldsymbol{v}) + \nabla \cdot (k \nabla T), \tag{1c}$$

where the components of the stress tensor $\boldsymbol{\tau}$ are $\boldsymbol{\tau}_{ij} = 2\mu e_{ij} - \frac{2}{3}\mu \delta_{ij} \nabla \cdot \boldsymbol{v}$ and $e_{ij} = \frac{1}{2}(\partial_j u_i + \partial_i u_j)$ are the components of the strain tensor $\boldsymbol{e}$.

For a two-dimensional flow of a perfect gas having a velocity vector $\boldsymbol{v} = (u, v)$ the above system of conservation equations reduces to the following form:

$$\rho_t + (\rho u)_x + (\rho v)_y = 0, \tag{2a}$$

$$(\rho u)_t + (\rho u^2 + p)_x + (\rho uv)_y = F_1, \tag{2b}$$

$$(\rho v)_t + (\rho uv)_x + (\rho v^2 + p)_y = F_2, \tag{2c}$$

$$E_t + [(E + p)u]_x + [(E + p)v]_y = uF_1 + vF_2 + Q + (kT_x)_x + (kT_y)_y, \tag{2d}$$

where

$$F_1 = 2(\mu u_x)_x + [\mu(u_y + v_x)]_y - \tfrac{2}{3}[\mu(u_x + v_y)]_x, \tag{3a}$$

$$F_2 = [\mu(u_y + v_x)]_x + 2(\mu v_y)_y - \tfrac{2}{3}[\mu(u_x + v_y)]_y, \tag{3b}$$

$$Q = \tfrac{2}{3}\mu\left((u_x - v_y)^2 + u_x^2 + v_y^2\right) + \mu(u_y + v_x)^2. \tag{3c}$$

The following relations are also used:

$$E = \frac{p}{\gamma - 1} + \tfrac{1}{2}\rho(u^2 + v^2), \quad T = \frac{p}{\rho R}, \quad \mu = \mu_0 \left(\frac{T}{T_0}\right)^{0.648}, \quad k = \frac{\mu}{(\gamma - 1)Pr}.$$

The solution of the above system of partial differential equations is completely determined by the parameters: $D, \theta_w, \gamma, a_0, \rho_0, \mu_0, T_0$ and Prandtl number Pr, where a subscript 0 denotes the initial state of the quiescent gas ahead of the propagating incident shock wave. These parameters enable one to define a unique combination of parameters that has the dimension of length, namely, $a_0^{-1}\rho_0^{-1}\mu_0$. Therefore, the problem does not have self-similar solutions that depend solely on x/t and y/t.

Let us now change the formulation of the problem by assuming that the dynamic viscosity μ_0 varies linearly with time, i.e. $\mu_0 = \kappa_0 t$, where the time is measured from the moment that the incident shock wave reached the leading edge of the reflecting wedge. In this case the governing parameters are $D, \theta_w, \gamma, a_0, \rho_0, \kappa_0, T_0$ and Pr. Unlike the previous case, a combination of parameters that has the dimension of length cannot be defined by these parameters. Thus in this formulation the problem does not have a characteristic length, and hence it allows self-similar solutions. The set of governing non-dimensional parameters for this formulation of the problem is

$$M_i = \frac{D}{a_0}, \quad \theta_w, \quad \gamma, \quad Pr, \quad \frac{\rho_0 a_0^2}{\kappa_0}.$$

The last non-dimensional parameter can be rewritten as

$$\frac{\rho_0 a_0^2}{\kappa_0}\frac{M_i}{\cos\theta_w} = \frac{\rho_0 a_0}{\kappa_0 t}\frac{Dt}{\cos\theta_w} = \frac{\rho_0 a_0}{\mu_0}L.$$

Here L is the distance OE that has been travelled by the incident shock wave along the reflecting wedge surface (see figure 1). Hereafter we will refer to this parameter, $\rho_0 a_0 L/\mu_0$, as the 'Reynolds number' of the problem in the self-similar viscous flow formulation and denote it as Re, i.e. $Re = \rho_0 a_0 L/\mu_0$.

Note that while in the real non-stationary viscous flow formulation (with a constant viscosity, μ_0) the Reynolds number grows with time, in the self-similar viscous flow formulation (with a viscosity that varies linearly with time, i.e. $\mu_0 = \kappa_0 t$) the Reynolds number is constant. Consequently, in the following we will refer to $Re = \rho_0 a_0 L/\mu_0$, in the real non-stationary formulation, as the *instantaneous Reynolds number*.

The W-modification of the Godunov method, which has second-order accuracy in both space and time (for details see Vasilev 1996), has been used as the basic numerical scheme for solving the above set of governing equations.

Curvilinear moving grids were used in the calculations. The initial position of the computational domain is shown in figure 1. The boundaries CT and TD were used to track the reflected, r, and the Mach stem, n, shock wave fronts during the calculations. The gas parameters behind the incident shock wave, i, were set as the initial conditions for the entire domain. In the production runs we employed the result of the previous computation as the initial condition for the next calculation in order to reduce CPU-time.

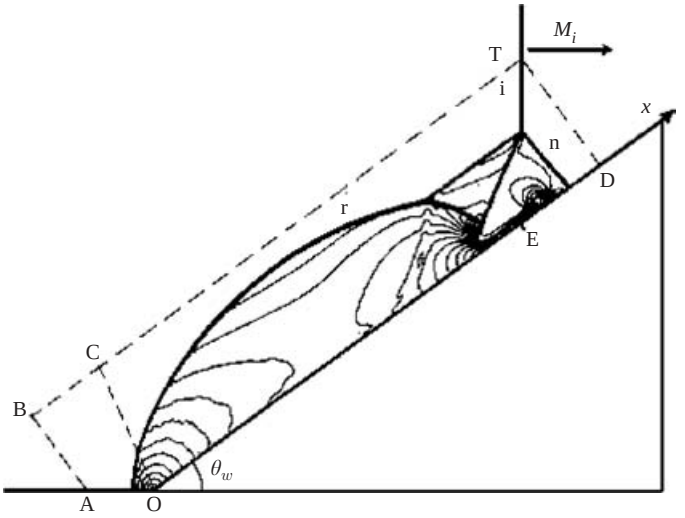

FIGURE 1. The boundaries of the moving computational domain. CT and TD are used for tracking the fronts of the reflected, r, and Mach, n, shock waves. M_i is the incident shock wave Mach number and θ_w is the reflecting wedge angle.

The following boundary conditions were imposed:

(i) zero slip velocity components along the wedge surface;

(ii) symmetry boundary conditions at the axis of symmetry upstream of the leading edge of the reflecting wedge;

(iii) $\partial p/\partial n = (\nabla \cdot \boldsymbol{\tau})_n$ where p is the pressure, $\boldsymbol{\tau}$ is the viscous stress tensor and n a direction normal to the reflecting wedge surface;

(iv) constant temperature that is equal to the initial temperature along the reflecting wedge surface;

(v) the parameters of the quiescent unperturbed gas at the boundary TD;

(vi) the parameters of the gas behind the incident shock wave for all the other boundaries.

The version of the W-modification of Godunov's scheme, which was previously employed by Ben-Dor *et al.* (1999), was modified to solve the Navier–Stokes equations using a splitting into physical processes. The viscous terms were approximated using an explicit scheme with central differences in space and a two-step Runge–Kutta method in time. At low Reynolds numbers at which one time step was used for the solution of inviscid gas equations several time sub-steps for the viscous terms were used. The number of time sub-steps required was determined by estimating a time step necessary for the stability of the marching method for the heat conduction equation. Thus, the Navier–Stokes solver employed had second-order accuracy both in space and time. In addition, a procedure for tracking the shock wave fronts and a mesh refinement technique near the triple point (for details see Henderson *et al.* 2003) were applied.

After each time step the length OE (figure 1) was used to normalize the coordinates of the mesh points. Thus, once the solution attained a self-similar state, the mesh and all the flow parameters became constant. The calculations were performed until the solution attained this state. The absolute value of both the time derivatives of the density and the trajectory angle of the triple point (node), were used as quantitative estimates of the degree of unsteadiness. The calculations showed that the latter

estimate was the most robust since the triple-point trajectory angle was found to be the slowest to attain the self-similar state. Note that renormalization of the mesh coordinates at each time step was performed only for convenience and did not affect the results of calculations.

In all the cases where the jets were stable, the self-similar state was attained with high accuracy. When the jet was unstable, the calculation times were two to three times longer than those with stable jets.

The majority of calculations were performed for an incident shock wave Mach number $M_i = 4.5$, and a wedge angle $\theta_w = 36^\circ$, using a 420×100 mesh. The mesh was refined by a factor 2 near the reflecting wedge surface in the region inside the boundary layer. Note that Henderson *et al.* (2003) presented calculations for an inviscid flow with exactly these values. The Reynolds number, $Re = \rho_0 a_0 L/\mu_0$, was changed in the range $500 \leqslant Re \leqslant 40\,000$. As was noted above, this parameter characterized the characteristic lengthscale of the flow.

In the final part of the paper a grid convergence of the numerical method and a comparison with an experimental result are presented for an incident shock wave Mach number $M_i = 3.22$, and a wedge angle $\theta_w = 32^\circ$.

3. Numerical results

3.1. *Self-similar viscous flow model*

The isopycnics (constant-density contours) in the vicinity of a Mach stem for a Mach reflection for the case of a self-similar viscous flow, for Reynolds numbers in the range $500 \leqslant Re \leqslant 2200$ are shown in figure 2. The following characteristic features of the flow field should be noted:

(i) in all the cases calculated the solutions obtained are stable, i.e. they are stationary in a moving frame of reference;

(ii) the Mach stem is significantly curved near the wall due to the effect of the boundary layer that is clearly visible behind its front;

(iii) the height of the Mach stem and the triple-point trajectory angle strongly increase when the Reynolds number increases;

(iv) the contact surface (slipstream) emanating from the triple point and the jet near the wall are strongly smeared by the viscosity;

(v) at $Re < 2000$ the wall-jet is attached to the boundary layer, and there is a counterclockwise-rotating vortex at its end;

(vi) at $Re \geqslant 2000$ the jet is lifted above the boundary layer, and a clockwise rotating suspended vortex is formed at its end.

Feature (vi) is clearly visible in figure 3 where the streamlines in a self-similar frame of reference are shown for $Re = 2000$. The streamlines of the fluid particles that passed through the reflected shock wave and those that passed through the Mach stem are shown separately in parts (*a*) and (*b*) of the figure, respectively. An additional vortex between the wall-jet and the contact surface is clearly seen (see (*b*)) apart from the above-mentioned suspended vortex. Only those fluid particles that passed through the upper part (about the upper third part) of the Mach stem are seen to flow into this vortex.

It was noted above when figure 2 was discussed that a decrease of the Reynolds number results in a decrease in the slope of the trajectory of the triple point. Thus one can ask whether the Mach stem disappears at $Re = 0$ or at $Re > 0$. The model which has been employed in the present study does not provide an exact answer to this question for the following two reasons. The first is that the shock wave tracking

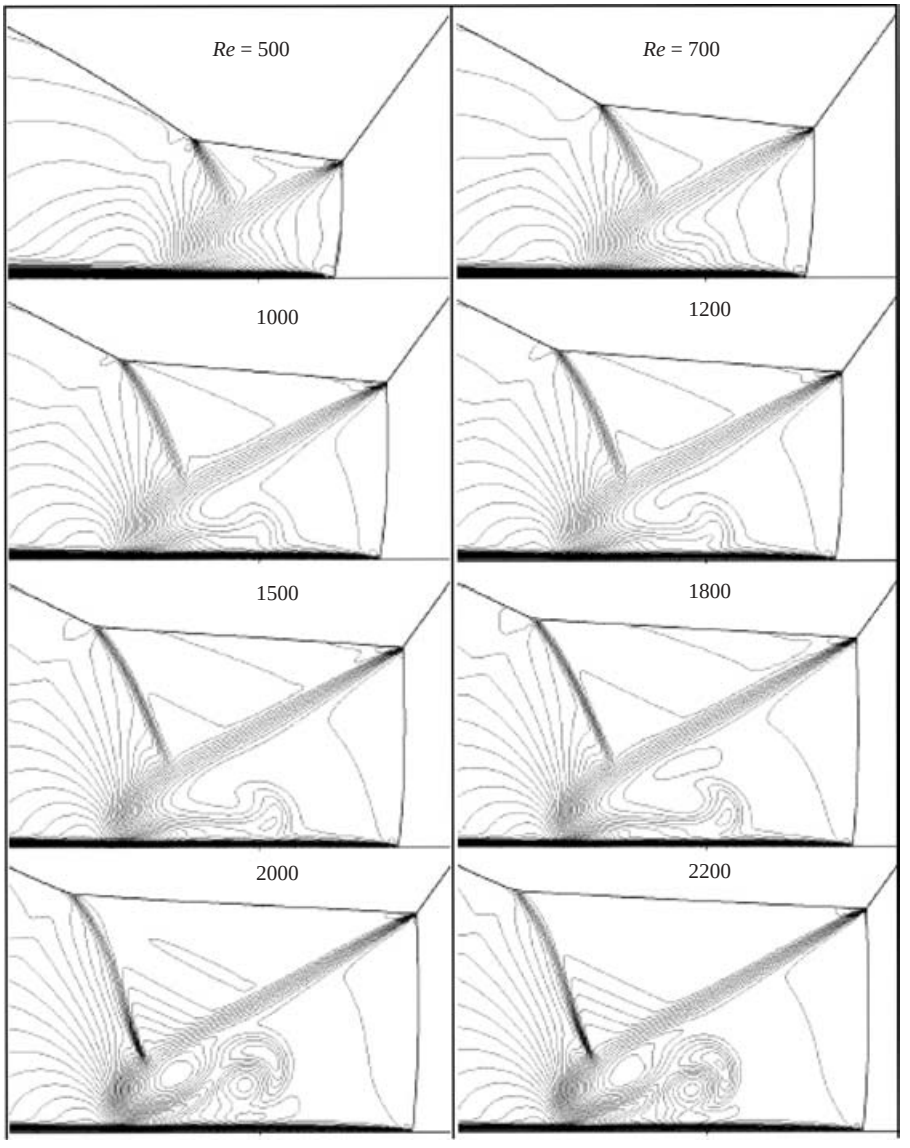

FIGURE 2. Isopycnics near the Mach stem for the self-similar viscous flow model for different Reynolds numbers. The flow fields are stable.

technique that used in the present numerical investigation implies that the shock wave fronts are discontinuities, i.e. infinitely thin. However, it is well-known that at sufficiently small Reynolds numbers the finite width of the shock wave cannot be neglected. The second reason is that calculations of the viscous effects using an explicit scheme, as has been done in the present study, require prohibitively high CPU-time when the Reynolds number and the cell size become smaller in the vicinity of the Mach stem. However, calculations performed with a small increment in the Reynolds number enable one to extrapolate the results to $Re \rightarrow 0$.

The calculated dependences of the slope of the triple-point trajectory and the Mach number of the Mach stem near the wall on the Reynolds number, for $Re \geqslant 350$, for the case of a self-similar viscous flow model are shown in figure 4. Extrapolation

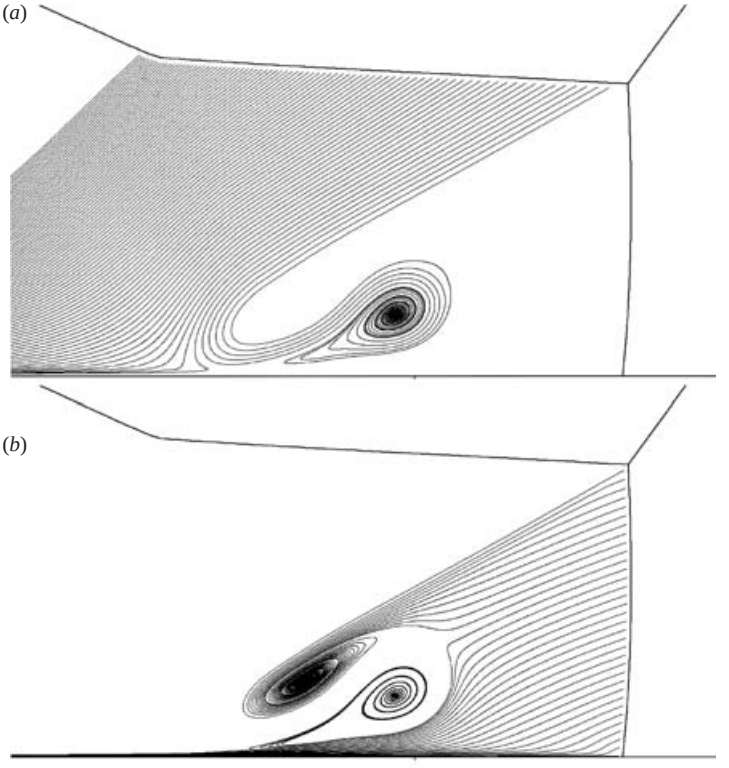

FIGURE 3. The streamlines that passed through (*a*) the reflected and (*b*) Mach stem shock waves for the self-similar viscous flow model with $Re = 2000$.

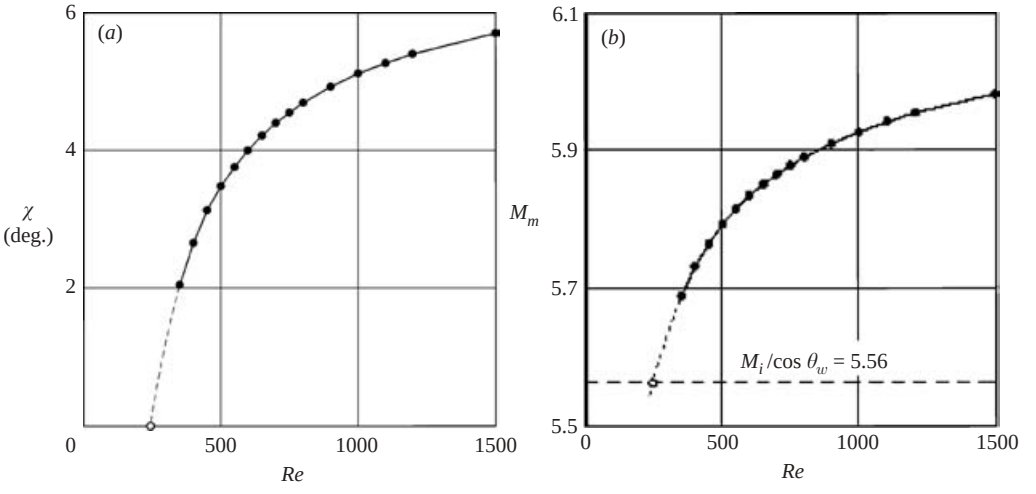

FIGURE 4. Dependence of (*a*) the triple-point trajectory angle and (*b*) the Mach number of the Mach stem near the reflecting wedge surface on the Reynolds number. The dashed lines denote extrapolation of the numerical results into the lower-Reynolds-numbers regime.

of the results to smaller Reynolds numbers, shown by dashed lines, shows that the Mach stem disappears at a finite Reynolds number $Re \approx 250$. At this Reynolds number the slope of the triple-point trajectory vanishes and the Mach number of the Mach stem attains the value of $M_i / \cos\theta_w$, which corresponds to a regular reflection. Consequently, a Mach reflection does not occur at small Reynolds numbers in the self-similar viscous flow model.

Note that the self-similar viscous flow model underestimates the viscous effects compared with the real non-stationary flow. Therefore in the full non-stationary formulation these effects will be more pronounced. At the early stage of the reflection of the shock wave from the wedge, when the instantaneous Reynolds number is not high, there is no Mach stem and it will appear only after some finite time. Thus, there is a delay in the appearance of the Mach reflection. Since in order to be observed experimentally, the Mach stem must attain a height of the order of 1–2 mm the delay in the appearance of the Mach reflection could be quite significant (for more details regarding the delay in the appearance of the Mach reflection see Henderson *et al.* 2001; Adachi, Sakurai & Kobayashi 2002).

The isopycnics for the self-similar viscous flow model with characteristic sizes that correspond to Reynolds numbers in the range $2500 \leqslant Re \leqslant 15\,000$ are shown in figure 5. The principal characteristic feature in all the cases is that the stationary flows are unstable. The suspended vortex at the end of the wall-jet oscillates between the contact surface (slipstream) and the reflecting wall surface.

Various phases of this oscillation phenomenon are clearly visible in the frames of figure 6, where the temporal evolution of the vortex oscillations for $Re = 3500$ is shown. The time interval between the frames, in figure 6, is equal to 0.1 of the oscillation period. It can be seen that the oscillations affect the shape of the second Mach stem, and that the bottom part the second Mach stem is essentially non-stationary. An inspection of frames (*a*) and (*k*) and (*b*) and (*l*), which are practically identical, suggests that an almost perfect periodicity of the oscillations exists in this case.

Note that the W-modification of the Godunov method has already been used for investigating pulsations in a self-similar flow and it was verified against other methods of the Godunov type (Vasilev & Danilchuk 1996).

A quantitative estimate of the stationarity of the flow field was calculated using the discrete analogue of the residual (for more details see Vasilev 1998):

$$R_n = \frac{1}{S} \iint_S \frac{1}{\rho} \left| \frac{\partial \rho}{\partial t} \right| \mathrm{d}s,$$

where S is the domain occupied by the flow field. The behaviour of R_n on a logarithmic timescale for the developed oscillatory flows, for $Re = 3000$, 4500 and 6000, is shown in figures 7(*a*), 7(*b*) and 7(*c*), respectively. One unit on the logarithmic timescale corresponds to a real time interval during which the size of the flow field is doubled. It can be seen that at $Re = 3000$ (figure 7*a*) the oscillations are periodic and the period is close to unity, i.e. to the value of the flow size doubling time. At $Re = 4500$ (figure 7*b*) the subsequent oscillations have different shapes and a period doubling is observed, i.e. each second oscillation has the same shape (more precisely the period grows by a factor slightly larger than 2). At $Re = 6000$ (figure 7*c*) a second period doubling is observed, i.e. each fourth oscillation has the same shape. However, as can be clearly seen in the figure, exact periodicity is not observed. When the Reynolds number increases further the latter tendency remains, i.e. a period doubling occurs but

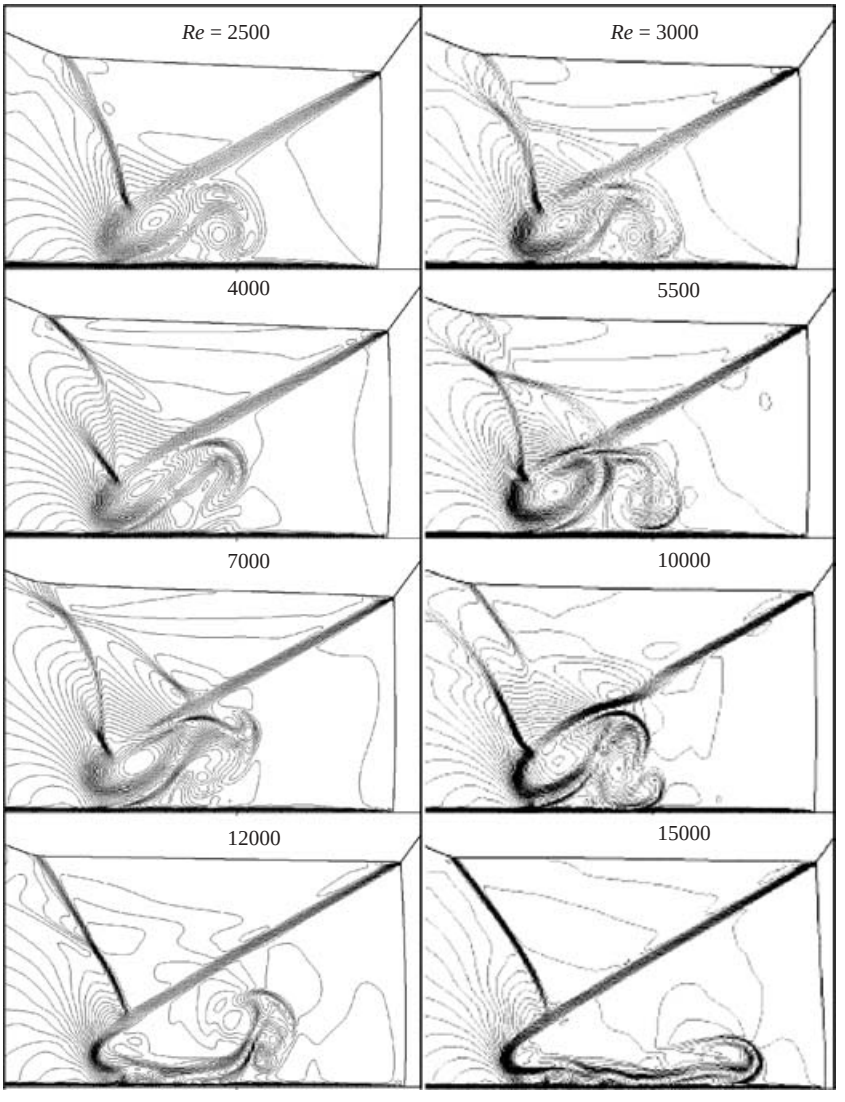

FIGURE 5. Isopycnics for the self-similar viscous flow model for different Reynolds numbers. The flow fields are unstable.

the repeatability of the oscillations is not as good. Thus a transition to non-periodic oscillations, i.e. a transition to a turbulent flow pattern in the wall-jet occurs.

At $Re > 10\,000$ (see figure 5) a qualitative change in the behaviour of the wall-jet is seen to take place. Almost the entire wall-jet is attached to the reflecting wall surface except for the vortex at its end. The end vortex performs non-periodic oscillations whereby a separation zone is formed at the end of the wall-jet due to its interaction with the boundary layer. Then a clockwise-rotating vortex is formed; the initial stage of this process is seen in figure 5 at $Re = 15\,000$. This vortex separates from the wall surface together with the trailing part of the wall-jet and the stream carries it to the leading part of the wall-jet. The initial stage of this process is seen in figure 5 at $Re = 12\,000$. Then all the cycles repeat. Note that this is the main difference between the behaviour of the wall-jets in the viscous and the inviscid flow models. In the

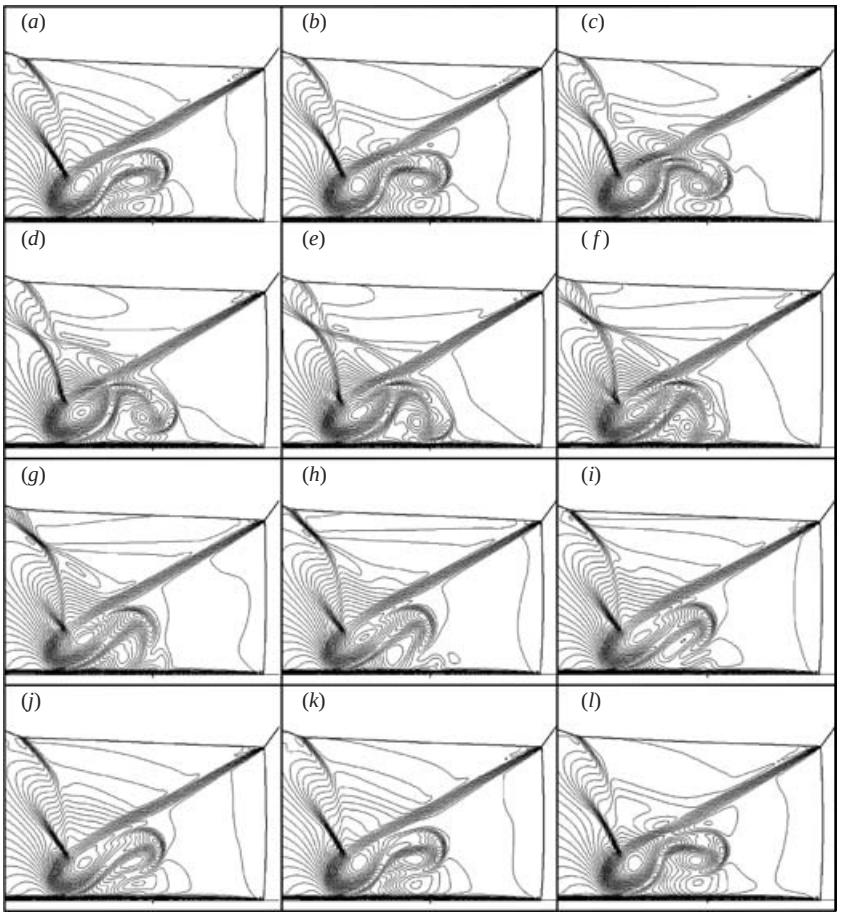

FIGURE 6. Isopycnics with periodic oscillations of a suspended end vortex in a jet for an unstable self-similar viscous flow model with $Re = 3500$.

latter model the oscillations of the wall-jet are not accompanied by a separation of its trailing part.

3.2. *Non-stationary viscous flow model*

In order to study truly non-stationary viscous flows a self-similar solution at $Re = 500$ was selected as an initial condition. In the calculations with a moving mesh the incident shock wave and the Mach stem were located initially to the right of the leading edge of the reflecting wedge, and the flow behind the Mach stem was inhomogeneous. Note that in the inviscid flow calculations the choice of the initial conditions was not important since in the case of pseudo-stationary flows, when oscillating flows were analysed, we were looking for the stationary solution or for a settled solution. Therefore in that case the calculations were performed until the solution 'forgot' the initial conditions, i.e. until the initial conditions ceased to affect the resulting solution. In the non-stationary problems the duration of the process (and, therefore, the calculation time) was determined by the problem, and we were also interested in knowing the intermediate states. Therefore, in this case the initial conditions were degenerate since they corresponded to $Re = 0$, and we wished to start from some small $Re > 0$. The calculations with small Reynolds numbers using explicit schemes

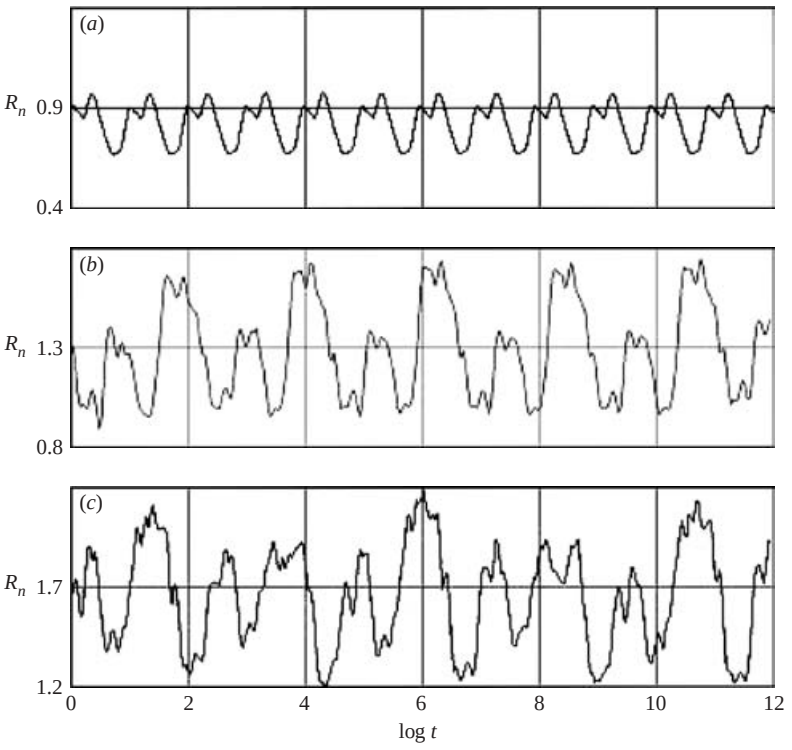

FIGURE 7. Oscillations of R_n for an unstable self-similar viscous flow vs. logarithm of the time for (*a*) $Re = 3000$, (*b*) $Re = 4500$, (*c*) $Re = 6000$.

required small time steps in order to secure the stability of the finite difference scheme. In this study our calculations started from $Re = 500$, and it was assumed that prior to this moment the flow developed as a self-similar viscous flow.

The time evolution of the wall-jet obtained using the truly non-stationary viscous flow model is shown in figure 8. It can be seen that at small instantaneous Reynolds numbers the solutions are more or less identical to those obtained using a self-similar approach (compare with figure 2). Only starting from a certain Reynolds number is the delay in the flow pattern with respect to a Reynolds number observed, i.e. similar solutions are obtained in the non-stationary viscous flow at larger instantaneous Reynolds numbers (note that a delay in the size is equivalent to a delay the time). The stage when the wall-jet is lifted above the reflecting wedge surface occurred considerably later than in the self-similar viscous flow model case (from $Re \approx 8000$).

There is also not enough time for the formation of the wall-jet with a suspended vortex as occurs in the flow field shown in figure 2 since during this time the instantaneous Reynolds number increases considerably, and the stage when the wall-jet is attached to the reflecting wedge surface begins (from $Re \approx 18\,000$). At large instantaneous Reynolds numbers the flow in the wall-jet is seen to be identical to that in the case of a self-similar viscous flow model with oscillations.

The quantitative differences between the self-similar and the truly non-stationary viscous flow cases can be seen in figure 9 where the dependence of the triple-point trajectory angle on the Reynolds number (i.e. the linear size which in the non-stationary flow case depends on the time, i.e. $Re = \rho_0 a_0 Dt/(\mu_0 \cos\theta_w)$) is shown. The curves with the black dots correspond to the case of a self-similar viscous flow model.

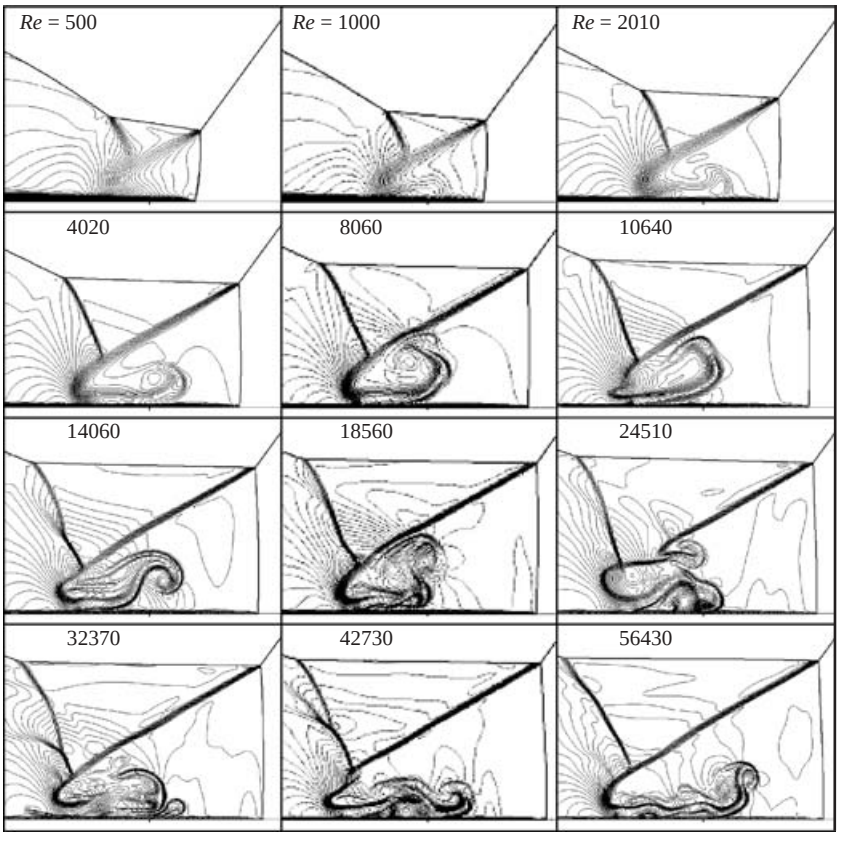

FIGURE 8. Temporal evolution of a jet for the non-stationary viscous flow model. The instantaneous Reynolds number is shown on the frames.

The upper curve corresponds to the maximum value of the triple-point trajectory angle at the stage where the oscillations began while the lower curve corresponds to the minimum value of the triple-point trajectory angle. These curves merge into a single curve at the point where the oscillations disappear, and hence it corresponds to the stable self-similar solution. The solid line without the black dots shows the case of the truly non-stationary viscous flow model. Clearly, in this case the triple-point trajectory angle and the height of the Mach stem grew more slowly than in the case of the self-similar viscous flow model.

Similar results for the Mach number of the foot of the Mach stem at the reflecting wall surface are shown in figure 10. Here the situation is somewhat different, i.e. in the case of a truly non-stationary viscous flow the velocity of the Mach stem grows faster than in the self-similar viscous flow case. The reason is associated with the non-stationary effects. In a self-similar flow the Mach stem velocity, $D_{m,ss}$, is proportional to its coordinate, while in a non-stationary flow the Mach stem velocity, D_m, equals the time derivative of the coordinate:

$$D_{m,ss} = \frac{X_m}{t} = \frac{X_m}{L}\frac{D}{\cos\theta_w}, \qquad D_m = \frac{d\,X_m}{\mathrm{d}t}.$$

In a self-similar flow these values are equal. In a non-stationary flow they are different and the difference between them characterizes the magnitude of non-self-similarity.

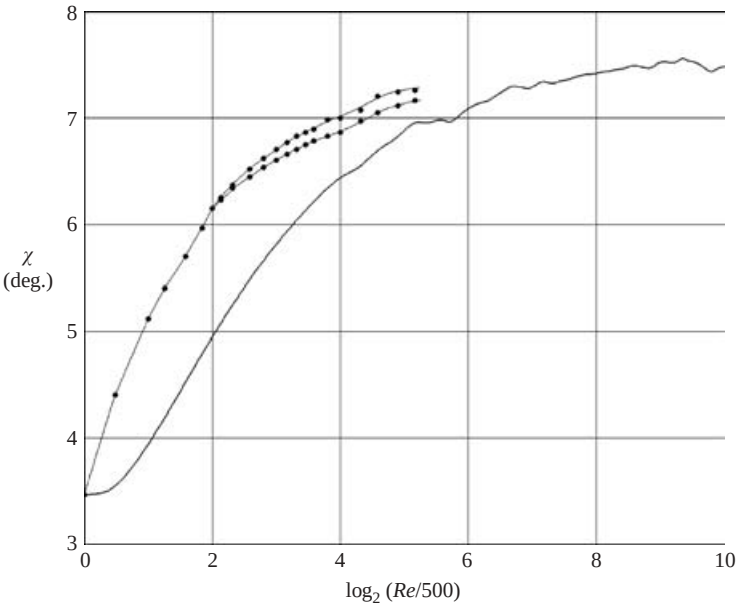

FIGURE 9. Slope of the trajectory of a triple point versus the instantaneous Reynolds number (vs. linear dimension) for the self-similar (curves with black dots) and non-stationary (plain solid lines) viscous flow models.

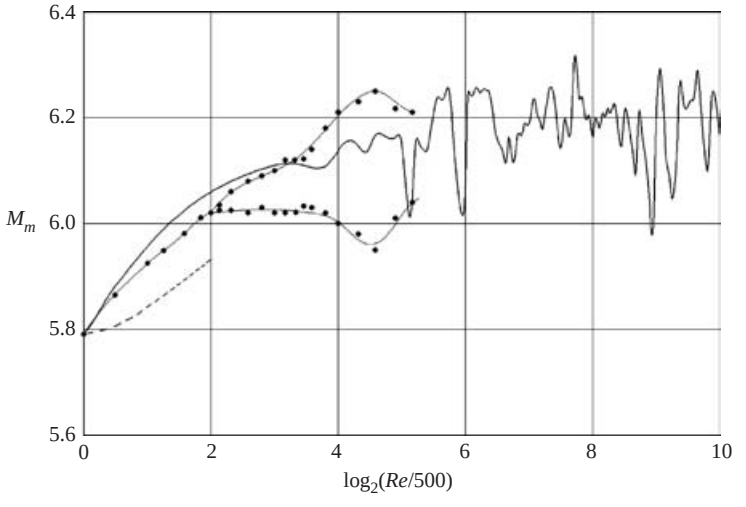

FIGURE 10. Mach number of the Mach stem near the wall versus the instantaneous Reynolds number (vs. linear dimension) for the self-similar (curves with black dots) and non-stationary (plain solid lines) viscous flow models. Dashed line is the average velocity of the stem in the non-stationary viscous flow.

In a non-stationary flow $D_{m,ss}$, in a time t, is the average velocity of the Mach stem in the time interval $[0, t]$. This average velocity for the non-stationary viscous flow is shown in figure 10 as a dashed line. It is seen that the average velocities in the self-similar flow and in the non-stationary flow correlate well with the triple-point trajectory angles. But the actual Mach stem velocity in the truly non-stationary viscous

flow is larger than the Mach stem velocity in the self-similar viscous flow due to the non-stationary effect. Indeed, this can be easily shown analytically assuming a straight Mach stem. The difference between the self-similar and non-stationary viscous flow velocities of the foot of the Mach stem is proportional to the time derivative of the triple-point trajectory angle, which is positive in the non-stationary viscous flow case:

$$X_m = Dt\frac{\sin\chi}{\cos(\chi+\theta_w)},$$

$$D_m = \frac{\mathrm{d}X_m}{\mathrm{d}t} = D\frac{\sin\chi}{\cos(\chi+\theta_w)} + Dt\frac{\cos\theta_w}{\cos^2(\chi+\theta_w)}\frac{\mathrm{d}\chi}{\mathrm{d}t}.$$

The additional term (with the derivative $\mathrm{d}\chi/\mathrm{d}t$) is the reason for the higher velocity of the foot of the Mach stem in the non-stationary viscous flow case while for a triple-point trajectory angle the situation is the opposite.

It can be clearly seen in figure 10 that the destabilization of the non-stationary flow occurs much later than in the self-similar viscous flow case. The delay time equals 2 units, i.e. if the self-similar viscous flow is stable until it reaches the size L, the non-stationary flow is stable at least until it reaches the size $4L$.

4. Comparison with experiments and the grid convergence of the computations

A correct comparison between the computational and experimental results can be conducted only at low instantaneous Re, i.e. at the stage when the jetting instability is not the dominating factor. Unfortunately, information in the scientific literature about such experiments is scarce. One example is illustrated in Bazhenova *et al.* (1986, p. 62). A scaled-up fragment of the schlieren photograph of this experiment is shown in figure 11(*a*). The incident shock wave propagated in nitrogen with Mach number $M_i = 3.22$, and wedge angle $\theta_w = 32^\circ$; the pressure ahead of the incident shock wave was $p_0 = 5$ torr (i.e. 0.00657 atm). Owing to the low pressure the instantaneous Reynolds number for the experimental snapshot is rather small $Re \approx 12\,000$–$13\,000$. The calculations were conducted using the non-stationary viscous flow model on a grid 800×240. The numerical density contour lines for $Re = 12\,500$ are shown in figure 11(*b*). By the time the photograph was taken the jet had already been lifted above the boundary layer. At a later time the jet instability process began to develop. Overall there is very good agreement between the experimental result and the numerical simulation regarding the location and shapes of both the shock waves and the jet configurations.

The effect of mesh refinement on the accuracy of the calculations (i.e. the convergence on a grid) is demonstrated in figure 12. Isopycnics from the self-similar viscous flow model for two different grids (with factor 2 difference in each direction) are shown. The incident shock wave Mach number is $M_i = 3.22$, the wedge angle is $\theta_w = 32^\circ$, and the Reynolds number is $Re = 4000$. The Reynolds number was selected so that the jet had already been lifted above the boundary layer but still preserved its stability (for example, see figure 2, $Re = 2000$ and 2200). It is evident that the isopycnics are practically identical in spite the fact that grids are different. This verifies both the convergence of the numerical method and sufficient grid resolution.

5. Summary and conclusions

The wall-jetting effect in Mach reflections in viscous pseudo-steady flows (as obtained in shock tubes) has been investigated numerically. The W-modification of Godunov's scheme was modified to solve the Navier–Stokes equations by splitting

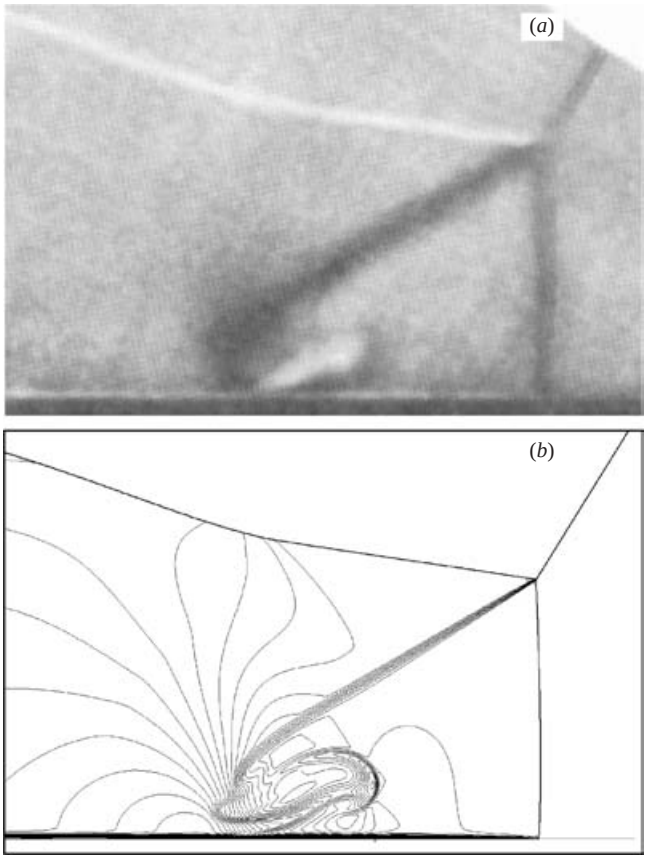

FIGURE 11. Comparison between an experiment (*a*), and the corresponding numerical simulation (*b*), for the non-stationary viscous flow. The incident shock wave Mach number is $M_i = 3.22$, the wedge angle is $\theta_w = 32^\circ$. The instantaneous Reynolds number is $Re = 12\,500$.

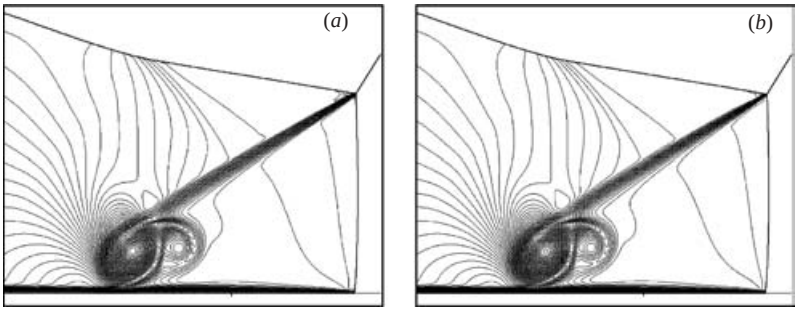

FIGURE 12. Isopycnics for the self-similar viscous flow model, calculated on two different grids, for $M_i = 3.22$, $\theta_w = 32^\circ$ and $Re = 4000$. (*a*) 500×150 grid; (*b*) 1000×300 grid. The density contour increment is $\Delta\rho/\rho_0 = 0.07$.

into physical processes. The viscous terms were approximated using an explicit scheme with central differences in space and a two-step Runge–Kutta method in time. Two analytical models were considered. The first was a self-similar viscous flow model

with a flow field of characteristic size L, and assuming that as the characteristic size grew from 0 to L, the viscosity of the gas ahead of the shock wave varied from 0 to μ_0. Consequently, the flow could be made self-similar by using the parameter $Re = \rho_0 a_0 L/\mu_0$. The second was a real non-stationary viscous flow, in which the molecular viscosity during the growth of the characteristic size from 0 to L remained constant and was equal μ_0. As a result the viscous effects were only partially accounted for in the self-similar viscous flow model in comparison to a real non-stationary viscous flow model, since they were smaller in the former case.

It was found in the case of the self-similar viscous flow model that:

(i) in all cases at $Re < 2000$ the solutions obtained were stable;

(ii) the Mach stem was significantly curved near the wall;

(iii) the height of the Mach stem and the triple-point trajectory angle strongly increased when the Reynolds number increased;

(iv) the delay in the appearance of the Mach reflection suggested recently by various investigators has been observed;

(v) the contact surface emanating from the triple point and the jet near the wall were strongly smeared by the viscosity;

(vi) at $Re < 2000$ the wall-jet was attached to the boundary layer, and there was a counterclockwise-rotating vortex at its end;

(vii) at $Re \geqslant 2000$ the jet was lifted above the boundary layer, and a clockwise-rotating suspended vortex was formed at its end.

(viii) at $Re \geqslant 2200$ the steady flow lost stability. The suspended vortex at the end of the wall-jet oscillated between the contact surface (slipstream) and the reflecting wall surface.

In the case of the non-stationary viscous flow model it was found that:

(i) the solutions at small Reynolds numbers were very similar to those obtained using the self-similar viscous flow model case;

(ii) the stage when the wall-jet was lifted above the reflecting wedge surface occurred considerably later than for the self-similar viscous flow model;

(iii) the triple-point trajectory angle and the height of the Mach stem grew more slowly than for the self-similar viscous flow model.

(iv) the velocity of the Mach stem was found to grow faster than for the self-similar viscous flow.

(v) the destabilization of the non-stationary flow occurs much later than for the self-similar viscous flow.

The present investigation complements our previous investigation of the wall-jetting effect in Mach reflection in inviscid pseudo-steady flows (Henderson *et al.* 2003).

This study was conducted under the auspices of the Dr Morton and Toby Mower Chair of Shock Wave Studies.

REFERENCES

Adachi, T., Sakurai, A. & Kobayashi, S. 2002 Effect of boundary layer on Mach reflection over a wedge surface, *Shock Waves* **11**, 271–278.

Bazhenova, T. V., Gvozdeva, L. G., Lagutov, Yu. P., Liahov, V. N., Faresov, Yu. M. & Fokeev, V. P. 1986 *Non-stationary Interactions of Shock Waves and Detonation Waves in Gases*. Nauka, Moscow (in Russian).

Ben-Dor, G. 1991 *Shock Wave Reflection Phenomena*. Springer.

Ben-Dor, G., Elperin, T., Li, H. & Vasilev, E. 1999 The influence of downstream pressure on the shock wave reflection phenomenon in steady flows. *J. Fluid Mech.* **386**, 213–232.

Henderson, L. F., Takayama, K., Crutchfield, W. Y. & Itabashi, S. 2001 The persistence of regular reflection during strong shock diffracting over rigid ramps. *J. Fluid Mech.* **431**, 273–296.

Henderson, L. F., Vasilev, E. I., Ben-Dor, G. & Elperin, T. 2003 The wall-jetting effect in Mach reflection: theoretical consideration and numerical investigation. *J. Fluid Mech.* **479**, 259–286.

Jones, D. M., Moira, P., Martin, E. & Thornhill, C. K. 1951 A note on the pseudo-stationary flow behind a strong shock wave diffracted or reflected at a corner. *Proc. R. Soc. Lond.,* A **209**, 238–248.

Li, H. & Ben-Dor, G. 1995 Reconsideration of pseudo-steady shock wave reflections and the transition criteria between them. *Shock Waves* **5**, 59–73.

Vasilev, E. I. 1996 A W-modification of Godunov's method and its application to two-dimensional non-stationary flows of a dusty gas. *Comput. Math. Math. Phys.* **36**, 101–112. (Translation from *Zh. Vychisl. Mat. Mat. Fiz.* **36**(1), 122–135.)

Vasilev, E. I. 1998 Instability of self-similar ideal gas flows with shock waves. *Fluid Dyn.* **33**, 604–611. (Translation from *Izv. RAN, Mekh. Zhidk. i Gaza* **4**, 166–175.)

Vasilev, E. I. & Danilchuk, E. V. 1996 Numerical simulation and research of the gas flow through expanding slit. *Rep. VGPU,* N1-96. Volgograd, Russia (in Russian).